ACES Asian Chemical Editorial Society

DOI: 10.1002/asia.201600370

CHEMISTRY AN ASIAN JOURNAL Communication

Layered Compounds

Superionic Conduction in Co-Vacant P2-Na_xCoO_2 Created by Hydrogen Reductive Elimination

Kenichi Kato,*[a, b] Hidetaka Kasai,[a, b, c] Akihiro Hori,[a, d] Masaki Takata,[a, e] Hiroshi Tanaka,[f] Susumu Kitagawa,[a, d] Akira Kobayashi,[g] Nobuki Ozawa,[b, g, h] Momoji Kubo,[g, h] Hidekazu Arikawa,[b, i] Tatsuya Takeguchi,[b, i] Masaaki Sadakiyo,[b, j] and Miho Yamauchi[b, j]

Abstract: The layered P2-Na_xMO_2 (M: transition metal) system has been widely recognized as electronic or mixed conductor. Here, we demonstrate that Co vacancies in P2-Na_xCoO_2 created by hydrogen reductive elimination lead to an ionic conductivity of 0.045 $S\,cm^{-1}$ at 25 °C. Using in situ synchrotron X-ray powder diffraction and Raman spectroscopy, the composition of the superionic conduction phase is evaluated to be $Na_{0.61}(H_3O)_{0.18}Co_{0.93}O_2$. Electromotive force measurements as well as molecular dynamics simulations indicate that the ion conducting species is proton rather than hydroxide ion. The fact that the Co-stoichiometric compound $Na_x(H_3O)_yCoO_2$ does not exhibit any significant ionic conductivity proves that Co vacancies are essential for the occurrence of superionic conductivity.

The P2-type Na_xMO_2 (M: transition metal) system has experienced a renewed interest in terms of the application to cathode materials for rechargeable Na-ion batteries, which are expected as the alternative to rechargeable Li-ion batteries owing to the sodium abundance on earth.[1–3] The electrochemical properties depend on the Na ordering and vacancies patterns as well as the Na concentrations.[4–8] In the P2-type layered structure, Na cations occupy two prismatic sites surrounded by six oxygen atoms from MO_2 anions.[9,10] Among a number of P2-type oxides, Na_xCoO_2 has been intensively studied since it has been found to exhibit a variety of physical properties such as large thermoelectric properties[11] and superconductivity[12] in addition to electrochemical properties.[1] The thermoelectric properties have been considered to depend on oxygen vacancies.[13,14] However, whether oxygen vacancies exist is controversial.[15,16] Furthermore, Vengust et al.[17] have proposed that the influence of Co vacancies rather than oxygen vacancies on physical parameters should be reconsidered based on their experimental studies. The P2 single phase can be obtained in the *x* range from 0.55 to 0.88 at the synthesis temperatures between 650 and 900 °C.[18] The formation of CoO has been found during Na_xCoO_2 synthesis below 800 °C under an Ar atmosphere and above 930 °C in air, and consequently the formation of Co vacancies is predictable to be ac-

[a] Dr. K. Kato, Dr. H. Kasai, Dr. A. Hori, Prof. Dr. M. Takata, Prof. Dr. S. Kitagawa
RIKEN SPring-8 Center
1-1-1 Kouto, Sayo-cho, Sayo-gun, Hyogo 679-5148 (Japan)
E-mail: katok@spring8.or.jp

[b] Dr. K. Kato, Dr. H. Kasai, Dr. N. Ozawa, Dr. H. Arikawa, Prof. Dr. T. Takeguchi, Dr. M. Sadakiyo, Prof. Dr. M. Yamauchi
CREST, Japan Science and Technology Agency
4-1-8 Honcho, Kawaguchi, Saitama 332-0012 (Japan)

[c] Dr. H. Kasai
Faculty of Pure and Applied Sciences, TIMS, CiRfSE
University of Tsukuba
1-1-1 Tennodai, Tsukuba, Ibaraki 305-8571 (Japan)

[d] Dr. A. Hori, Prof. Dr. S. Kitagawa
Institute for Integrated Cell-Material Sciences
Kyoto University
Yoshida, Sakyo-ku, Kyoto 606-8501 (Japan)

[e] Prof. Dr. M. Takata
Institute of Multidisciplinary Research for Advanced Materials
Tohoku University
2-1-1 Katahira, Aoba-ku, Sendai 980-8577 (Japan)

[f] Prof. Dr. H. Tanaka
Department of Materials Science
Shimane University
1060 Nishi-kawatsu-cho, Matsue, Shimane 690-8504 (Japan)

[g] A. Kobayashi, Dr. N. Ozawa, Prof. Dr. M. Kubo
Graduate School of Engineering
Tohoku University
6-6-11 Aoba, Aramaki, Aoba-ku, Sendai 980-8579 (Japan)

[h] Dr. N. Ozawa, Prof. Dr. M. Kubo
Institute for Materials Research
Tohoku University
2-1-1 Katahira, Aoba-ku, Sendai 980-8577 (Japan)

[i] Dr. H. Arikawa, Prof. Dr. T. Takeguchi
Department of Chemistry and Bioengineering
Iwate University
4-3-5 Ueda, Morioka, Iwate 020-8551 (Japan)

[j] Dr. M. Sadakiyo, Prof. Dr. M. Yamauchi
International Institute for Carbon-Neutral Energy Research
Kyushu University
744 Motooka, Nishi-ku, Fukuoka 819-0395 (Japan)

Supporting information for this article can be found under http://dx.doi.org/10.1002/asia.201600370.

companied by a high Na concentration.[17] However, the Co-vacant phase has not been identified in detail. The CoO formation can be considered to be due to reductive elimination, since the oxidation state of Co in Na_xCoO_2 ranges from +3 to +4 depending on the Na concentration. In the present work, we have succeeded in adding proton superionic conductivity to the P2-Na_xMO_2 system by employing the reductive elimination by hydrogen at a temperature lower than the synthesis temperatures. The conductivity record we have established is 0.045 S cm^{-1} at 25 °C, a value comparable to that of the practically used proton conductor Nafion.

In Figure 1, the mass ratio of each crystal phase observed during a chemical procedure in P2-Na_xCoO_2 is plotted as a function of time. The procedure consists of two steps: the first one is the hydrogen gas flow at 260 °C for 12 min, and the second is the exposure to ambient air at a temperature of 27 °C and a relative humidity (RH) of 30% for about 10 h in the glass capillary cell (Figure S1, Supporting Information). The conditions for the hydrogen treatment are carefully optimized such that not only the P2-layered structure does not chemically decompose but also its peak intensities reach a maximum (Figure S2). Part of the in situ synchrotron X-ray powder diffraction (SXPD) patterns are shown in Figure S3. On the basis of the Rietveld analysis (Figures S4 and S5) of these data, the mass ratio of each crystal phase has been obtained as a function of the chemical reaction time. For convenience, the four Na_xCoO_2-related phases found in this study are sequentially numbered from first to fourth hereafter. Table 1 lists structural parameters of the four phases at their respective maximum ratios.

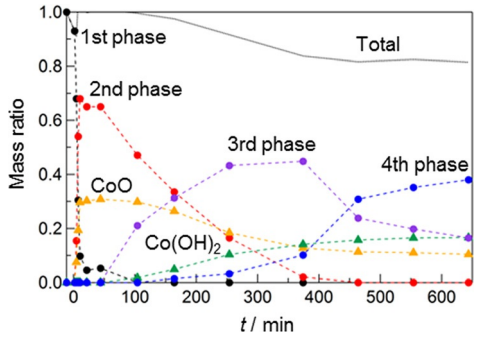

Figure 1. Time evolution of the mass ratios of crystal phases, which have been obtained by the Rietveld analysis of SXPD data under chemical reactions in Na_xCoO_2. The ratio of the first phase before the hydrogen treatment is set at 1.0.

Table 1. Structural parameters of the four Na_xCoO_2-related phases. All the phases belong to the space group $P6_3/mmc$.

Phase number (t min)	Composition	Oxidation number in Co[a]	a [Å]	c [Å]
1st (<0)	$Na_{0.69(1)}CoO_2$	3.31(1)	2.83189(1)	10.90026(8)
2nd (22)	$Na_{1.04(1)}Co_{0.875(3)}O_2$	3.38(3)	2.88326(1)	10.49537(7)
3rd (374)	$Na_{0.84(1)}Co_{0.931(4)}O_2$	3.39(3)	2.85612(2)	10.6933(1)
4th (644)	$Na_{0.79(2)}Co_{0.927(5)}O_2$	3.46(4)	2.84147(3)	10.8074(2)

[a] Oxidation numbers in Co were calculated based on the obtained compositions to maintain neutrality, assuming that nominal ionic valences in Na and O are +1 and −2, respectively.

We have found from the SXPD data that the first phase reacts with hydrogen at the elevated temperature into the second phase and CoO, the ratio of which is approximately 0.7 to 0.3. The Rietveld analysis has identified that the liberation of CoO forms Co vacancies of 12.5% in the second phase. In addition, a nearly 4% contraction in the lattice parameter c is observed in the second phase, which is consistent with a high Na concentration of almost 1.0. The creation of Co vacancies can best be understood such that a two-electron reductive elimination takes place by the hydrogen treatment. This is because the Co^{4+} ratio in the first phase is found from its oxidation number to be about 0.3, which corresponds to the ratio of CoO to the first phase. In fact, the oxidation number of the first phase is close to that of the second phase. The ratio of the second phase decreases with time, while that of the third phase increases. Furthermore, the third phase appears to be replaced by the fourth phase, suggesting that the third phase is an intermediate phase in this process. On the other hand, it has been observed that CoO reacts with H_2O in air to form $Co(OH)_2$.

The Rietveld refinement has identified that the Na concentrations of the third and fourth phases are lower than that of the second phase. It is predictable from these results that the second phase causes some reactions with H_2O in air. To confirm this prediction, Raman spectroscopy measurements have been conducted with circular disks before and after the hydrogen treatment, and after its treatment followed by humidification. Figure 2 shows Raman spectra of the three states at lower and higher wave numbers. Several intense peaks observed in the range from 500 to 700 cm^{-1} (Figure 2a) can be identified as those of Na_xCoO_2 with different compositions.[19] There is no doubt that the Raman laser is out of focus to any other phases such as CoO and $Co(OH)_2$. After the hydrogen treatment followed by the humidification, two peaks have been found around 1500 and 3000 cm^{-1} (Figure 2b), which correspond to the bending (H-O-H) and stretching (O–H) modes of oxonium ions (H_3O^+) in the Na layer,[20] respectively.

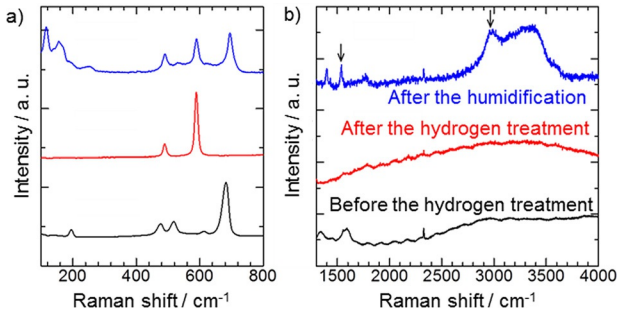

Figure 2. Raman spectra of Na_xCoO_2 before and after the hydrogen treatment, and after its treatment followed by humidification. Spectra at lower and higher wave numbers are shown in (a) and (b), respectively.

Additionally, the sharp and extremely broad peaks around 1400 and 3400 cm^{-1} may be due to the intercalation of H_2O between the Na and CoO_2 layers.[21] In contrast, no corresponding peaks are observed before and after the hydrogen treatment. These findings lead us to the conclusion that Co-vacant Na_xCoO_2 reacts with H_2O to form $Na_x(H_3O)_yCo_{1-\delta}O_2$.

Electrochemical measurements under humidity control have been done with and without hydrogen treatment to investigate electrical transport properties. Figure 3 shows the relative humidity (RH) evolution at 25 °C of ionic and electronic conductivities for Na_xCoO_2, which are obtained based on the measurements of alternating current (AC) and direct current (DC) conductivities, respectively. The hydrogen-treated disk is found to exhibit a significant frequency dependence of impedance between 1 Hz and 1 kHz (see Figure S6 for 50% RH), indicating that ionic conduction is predominant over electronic conduction. In contrast, the impedance of the untreated disk is virtually constant in the measurement range of frequency (see Figure S6 for 50% RH), in which case the real part of impedance is close to the DC resistance. Such a behavior is typical of electronic conduction. To estimate the ionic conductivity of the hydrogen-treated disk, semicircle components observed at higher frequency in Nyquist plots are fitted by the least-squares method for each humidity (Figure S7). At 28% RH, the ionic conductivity is comparable with the electronic conductivity, indicating mixed conductivity. A rapid decrease in electronic conductivity is observed at 30% RH. At humidities above 40% RH, however, the conductivities appear to reach a balance, resulting in a plateau. We have found that the ionic conductivity of the hydrogen-treated disk is as large as 0.045 $S\,cm^{-1}$ at 60% RH and 25 °C, while its electronic conductivity is suppressed to be of the order of 10^{-8} $S\,cm^{-1}$ under these conditions (Figure 3a). It is important to mention here that the humidified disk without the hydrogen pretreatment still remains an electronic conductor (Figure 3b).

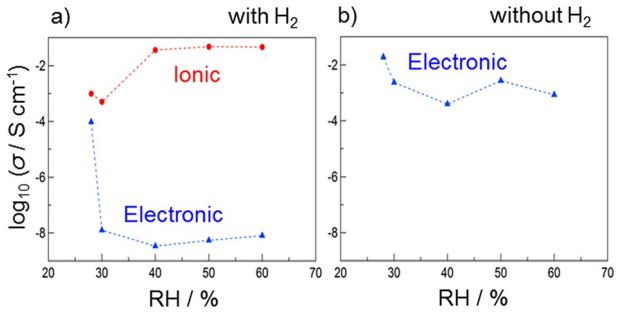

Figure 3. Ionic and electronic conductivities σ at 25 °C as a function of relative humidity (RH) on (a) the hydrogen-treated and (b) untreated Na_xCoO_2 disks. No significant ionic conductivity is observed in the untreated disk.

Here, the question arises as to what is the predominant ion species in the superionic conduction. In this case, there are two possibilities: one is a cation such as H^+ (H_3O^+) and the other is an anion such as OH^-. This is because the humidification (H_2O) treatment enhances the ionic conductivity as shown in Figure 3a. In order to investigate which ion is predominant, the electromotive force (EMF) has been measured using a water vapor concentration cell, which provides fundamental understanding on the conducting ion species for humidity-sensitive ionic conductors.[22] It has been recognized that the water vapor concentration cell with H^+ and OH^- conductive electrolytes indicates positive and negative EMF values, respectively.[22] We indeed observe positive and negative values in the commercial proton- and hydroxide-exchange membranes, respectively. The hydrogen-treated Na_xCoO_2 disk is found to show a positive value like the proton conductor (Figure 4).

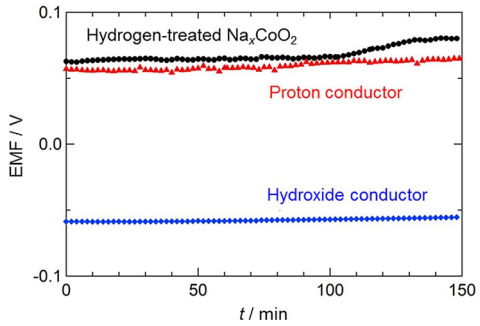

Figure 4. EMF measured by the water vapor concentration cell using the hydrogen-treated Na_xCoO_2 disk, a proton-exchange membrane (Nafion NRE-212), or a hydroxide-exchange membrane (Tokuyama A201) as the electrolyte.

Even though we have conducted systematic experimental studies as reported above, it remains unclear whether the P2-$Na_x(H_3O)_yCo_{1-\delta}O_2$ phase is really superionic-conductive due to the multicomponent system. To corroborate this point, here let us mention the contribution of other phases to ionic conductivity. The superionic conduction state found at 60% RH in Figure 3a corresponds to that at $t = 644$ min in Figure 1, since both conductivities and mass ratios reach a plateau. At this stage, there are four phases: fourth Na_xCoO_2, third Na_xCoO_2, $Co(OH)_2$ and CoO, which are in the approximate mass ratio of 4:2:2:1. That means the Na_xCoO_2-related phase occupies nearly 60% in the mass ratio at the superionic conduction state. Here we emphasize that $Co(OH)_2$ and CoO have been reported as an electronic conductor[23,24] and an insulator,[25,26] respectively. These findings indicate that superionic conduction in the composite system originates from the Co-vacant P2-Na_xCoO_2 phase. In contrast to the third Na_xCoO_2 phase, the fourth Na_xCoO_2 phase has a lower Na concentration as listed in Table 1. In other words, the fourth phase exhibits a higher ion exchange ratio of Na^+ into H_3O^+, which is the ionic conduction species as identified by the EMF measurement.

Raman spectra indicate the ion exchange of Na^+ for H_3O^+ in the Na layer, although the determination of exchange ratios for each Na site is clearly beyond the capability of the Rietveld method due to the identical electron number (10 for Na^+ and H_3O^+). Charge density analysis by the maximum entropy method (MEM) could provide a better knowledge on atomic sites such as disordering and anisotropic displacement.[27] An attempt to visualize experimental charge densities has been made for each Na_xCoO_2 phase. Charge densities of the first,

second, and fourth phases are shown in Figure S8. Unlike other phases (Figure S8a and S8b), in the case of the fourth phase (Figure S8c) the sites 3 and 1 in the Na layer appear to be disordered. This behavior in the fourth phase implies that H_3O^+ ions prefer the sites 3 and 1 over the site 2 in the superionic conduction phase. To corroborate this, the electron charge for each Na site, which is obtained from MEM charge densities, is plotted as a function of reaction time in Figure S9. In the case of the ordered site 2, the electron charge shows a gradual decrease with time. In contrast, the charge for the disorder site 1 is found to increase gradually with time, indicative of the occurrence of the ion exchange of Na^+ for H_3O^+. For the site 3, the charge decreases in the second and third phases but increases slightly in the fourth phase. Given that the increasing electron charge corresponds to that of H_3O^+, the composition of the fourth phase, that is, the superionic conduction phase, is considered to be $Na_{0.61}(H_3O)_{0.18}Co_{0.93}O_2$. The final structural parameters for all the Na_xCoO_2 phases are listed in Tables S1–S4, taking into account the disordered model.

Using the model based on the structural parameters for the superionic conduction phase in Table S4, molecular dynamics (MD) simulations have been performed to understand the behavior of ion conducting species. Figure 5c and 5d illustrate simulated trajectories of H, O and Na on the Na/H_3O layer (Figure 5a), respectively. H atoms appear to diffuse between the sites 2 and 3 (Figure 5c). On the other hand, the trajectory of O atoms is seen between the sites 1 and 2 (Figure 5d). In contrast to H and O atoms from H_3O, the motion of Na atoms is confined to sites 1 (invisible due to the CoO_2 model) and 2 (Figure 5d). Such dynamics can be best understood such that H atoms pass through the most vacant site 3, thereby maintaining a high mobility in the Na layer. In contrast, the site 3 is tight for the O and Na atoms due to their larger ionic radii, leading to their lower mobilities. It follows from this argument that the P2-$Na_x(H_3O)_yCo_{1-\delta}O_2$ phase is most likely a proton-based superionic conductor, which is consistent with the results of EMF measurements. Let us now evaluate the results of MD simulations, taking into account the electrostatic potentials[28] (Figure 5b) and electric fields (Figure S10) derived from MEM charge densities. The disordered sites found in the sites 1 and 3 distribute towards the site 2 due to electrostatic repulsions between the sites 1 and 3. Unlike the sites 1 and 3, the site 2 appears to be isolated from the point of view of electrostatic potentials. Electric fields in Figure S10b have clearly identified that every arrow between atoms converges on the potential local minimum found between the sites 1 and 2, as opposed to the case of the non-superionic conduction (first) phase in Figure S10a. The trace by electric fields is analogous to that by MD simulations in Figure 5c. It is important to mention here that Na in the site 2 is more likely to be localized as observed in Figure 5b, maintaining the robust layered structure and forming the ionic pathway like a honeycombed sublattice. A similar honeycombed diffusion pathway is predicted between the sites 1 and 2 in the P2-$Na_{0.56}CoO_2$ phase by first-principles MD simulations.[29] Considering the H_2O intercalation between the Na and CoO_2 layers as implied based on Raman spectroscopy, we propose the Grotthuss mechanism rather than the vehicle one for proton conduction in this system.

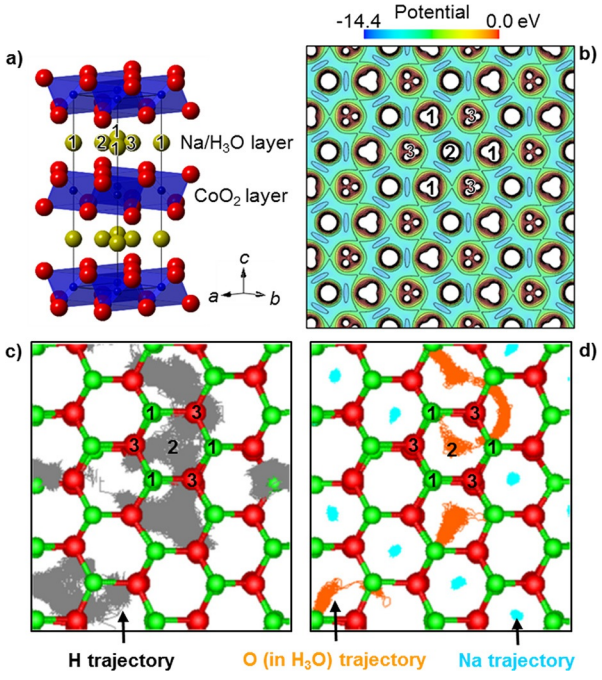

Figure 5. (a) The structure model for P2-$Na_x(H_3O)Co_{1-\delta}O_2$. (b) Electrostatic potentials on the Na layer obtained based on the MEM analysis of in situ SXPD data. Contour lines for potentials are drawn from −14.4 to 23.0 eV at intervals of 2.9 eV. Diffusion trajectories in the Na layer of (c) H and (d) O in H_3O and Na by MD simulations. Atomic site numbers 1, 2 and 3 for Na/H_3O are indicated in each figure. Green and red balls in (c) and (d) correspond to Co and O in CoO_2 projected on the Na layer, respectively.

In summary, the hydrogen reductive elimination has been employed to obtain the Co-vacant P2-Na_xCoO_2 phase. Consequently, we have found from electrochemical measurements that the electronic–superionic conduction transition occurs under elevated humidity at room temperature, in which case proton is predominant over hydroxide ion as the conducting species. In situ SXPD and Raman spectroscopy have revealed the creation of Co vacancies and the ion exchange of Na^+ for H_3O^+, respectively. Compared to electrochemical results, these findings lead us to the conclusion that creation of Co vacancies suppresses electronic conductivity and facilitates superionic conductivity. Based on MD simulations using the experimental structural model, a honeycombed sublattice for proton in the Na layer is proposed as the diffusion mechanism via the vacant Na sites. The results obtained in the present work clearly warrant further research on the pure single phase of P2-$Na_x(H_3O)_yM_{1-\delta}O_2$.

Acknowledgements

This work was supported by JSPS KAKENHI Grant Number 25871142. The synchrotron radiation experiments were performed at BL44B2 in SPring-8 with the approval of RIKEN (Proposal Noumbers 20110049, 20120073, and 20130090).

Keywords: layered compounds · molecular dynamics · reductive elimination · superionic conductivity · X-ray diffraction

[1] R. Berthelot, D. Carlier, C. Delmas, *Nat. Mater.* **2011**, *10*, 74 – 80.
[2] N. Yabuuchi, M. Kajiyama, J. Iwatate, H. Nishikawa, S. Hitomi, R. Okuyama, R. Usui, Y. Yamada, S. Komaba, *Nat. Mater.* **2012**, *11*, 512 – 517.
[3] M. Guignard, C. Didier, J. Darriet, P. Bordet, E. Elkaïm, C. Delmas, *Nat. Mater.* **2013**, *12*, 74 – 80.
[4] H. W. Zandbergen, M. Foo, Q. Xu, V. Kumar, R. J. Cava, *Phys. Rev. B* **2004**, *70*, 024101.
[5] M. Roger, D. J. P. Morris, D. A. Tennant, M. J. Gutmann, J. P. Goff, J.-U. Hoffmann, R. Feyerherm, E. Dudzik, D. Prabhakaran, A. T. Boothroyd, N. Shannon, B. Lake, P. P. Deen, *Nature* **2007**, *445*, 631 – 634.
[6] G. J. Shu, F. C. Chou, *Phys. Rev. B* **2008**, *78*, 052101.
[7] Y. S. Meng, Y. Hinuma, G. Ceder, *J. Chem. Phys.* **2008**, *128*, 104708.
[8] X. Li, X. Ma, D. Su, L. Liu, R. Chisnell, S. P. Ong, H. Chen, A. Toumar, J.-C. Idrobo, Y. Lei, J. Bai, F. Wang, J. W. Lynn, Y. S. Lee, G. Ceder, *Nat. Mater.* **2014**, *13*, 586 – 592.
[9] C. Fouassier, G. Matejka, J.-M. Reau, P. Hagenmuller, *J. Solid State Chem.* **1973**, *6*, 532 – 537.
[10] C. Delmas, C. Fouassier, P. Hagenmuller, *Physica B+C* **1980**, *99*, 81 – 85.
[11] I. Terasaki, Y. Sasago, K. Uchinokura, *Phys. Rev. B* **1997**, *56*, R12685 – 12687.
[12] K. Takada, H. Sakurai, E. Takayama-Muromachi, F. Izumi, R. A. Dilanian, T. Sasaki, *Nature* **2003**, *422*, 53 – 55.
[13] Y. Morita, J. Poulsen, K. Sakai, T. Motohashi, T. Fujii, I. Terasaki, H. Yamauchi, M. Karppinen, *J. Solid State Chem.* **2004**, *177*, 3149 – 3155.
[14] P. H. Tsai, T. Norby, T. T. Tan, R. Donelson, Z. D. Chen, S. Li, *Appl. Phys. Lett.* **2010**, *96*, 141905.
[15] I. R. Mukhamedshin, H. Alloul, *Phys. Rev. B* **2011**, *84*, 155112.
[16] S. Casolo, O. M. Løvvik, H. Fjeld, T. Norby, *J. Phys.: Condens. Matter* **2012**, *24*, 475505.
[17] D. Vengust, B. Jancar, A. Sestan, M. P. Svet, B. Budic, D. Suvorov, *Chem. Mater.* **2013**, *25*, 4791 – 4797.
[18] Y. Lei, X. Li, L. Liu, G. Ceder, *Chem. Mater.* **2014**, *26*, 5288 – 5296.
[19] H. X. Yang, Y. Xia, Y. G. Shi, H. F. Tian, R. J. Xiao, X. Liu, Y. L. Liu, J. Q. Li, *Phys. Rev. B* **2006**, *74*, 094301.
[20] H. Sakurai, M. Osada, E. Takayama-Muromachi, *Chem. Mater.* **2007**, *19*, 6073 – 6076.
[21] K. Takada, K. Fukuda, M. Osada, I. Nakai, F. Izumi, R. A. Dilanian, K. Kato, M. Takata, H. Sakurai, E. Takayama-Muromachi, T. Sasaki, *J. Mater. Chem. B* **2004**, *14*, 1448 – 1453.
[22] K. Tadanaga, Y. Furukawa, A. Hayashi, M. Tatsumisago, *Adv. Mater.* **2010**, *22*, 4401 – 4404.
[23] X.-P. Gao, S.-M. Yao, T.-Y. Yan, Z. Zhou, *Energy Environ. Sci.* **2009**, *2*, 502 – 505.
[24] C. Mondal, M. Ganguly, P. K. Manna, S. M. Yusuf, T. Pal, *Langmuir* **2013**, *29*, 9179 – 9187.
[25] J. van Elp, J. L. Wieland, H. Eskes, P. Kuiper, G. A. Sawatzky, F. M. F. de Groot, T. S. Turner, *Phys. Rev. B* **1991**, *44*, 6090 – 6103.
[26] T. Bredow, A. R. Gerson, *Phys. Rev. B* **2000**, *61*, 5194 – 5201.
[27] S. Kastbjerg, N. Bindzus, M. Søndergaard, S. Johnsen, N. Lock, M. Christensen, M. Takata, M. A. Spackman, B. B. Iversen, *Adv. Funct. Mater.* **2013**, *23*, 5477 – 5483.
[28] K. Kato, H. Tanaka, *Adv. Phys.: X* **2016**, *1*, 55 – 80.
[29] Y. Mo, S. P. Ong, G. Ceder, *Chem. Mater.* **2014**, *26*, 5208 – 5214.

Manuscript received: March 21, 2016
Final Article published: ■■ ▮▮, 0000

